

## Chirality-Dependent Transport Properties of Double-Walled Nanotubes Measured in Situ on Their Field-Effect Transistors

Kaihui Liu,<sup>†</sup> Wenlong Wang,<sup>†</sup> Zhi Xu,<sup>†</sup> Xuedong Bai,<sup>\*,†</sup> Enge Wang,<sup>\*,†</sup> Yagang Yao,<sup>‡</sup> Jin Zhang,<sup>‡</sup> and Zhongfan Liu<sup>†</sup>

Beijing National Laboratory for Condensed Matter Physics, Institute of Physics, Chinese Academy of Sciences, Beijing 100190, China, and Beijing National Laboratory for Molecular Sciences, State Key Laboratory for Structural Chemistry of Unstable and Stable Species, College of Chemistry and Molecular Engineering, Peking University, Beijing 100871, China

Received November 2, 2008; E-mail: xdbai@aphy.iphy.ac.cn; egwang@aphy.iphy.ac.cn

Double-walled carbon nanotubes (DWNTs), consisting of two coaxial tubes, possess mechanical properties and structural and thermal stability that are superior to single-walled carbon nanotubes.<sup>1,2</sup> Interestingly, they provide an ideal structure for the fabrication of nanoscale functional composites,<sup>3–5</sup> that is, chemical moieties are selectively introduced on the outer tubes as effective anchoring sites, while the inner tubes preserve their electronic properties. It is well-known that the electronic property of a carbon nanotube, which shows potential in nanodevices, depends sensitively on the atomic structure—uniquely indexed with the chiral indices ( $n$ ,  $m$ ). It is therefore of essential significance to be able to probe the chirality-resolved DWNTs so as to establish a direct correlation between the electrical transport properties and their chiral indices. Herein, we make progress on attaining this goal by building DWNT-based field-effect transistors (FETs) into a transmission electron microscope (TEM) through a new design, which allows for an accurate ( $n$ ,  $m$ ) assignment by electron diffraction (ED) on the same individual DWNTs that are electrically measured in situ inside the TEM. In this context, the transport properties of the chirality-resolved DWNTs are systematically investigated for all the four types of DWNTs, and the probe of inner tubes can also be achieved in situ.

Experiments were carried out in a JEOL 2010F field-emission-gun high-resolution TEM operated at 120 kV at room temperature and in a  $10^{-5}$  Pa vacuum. Since the conventional TEM specimen holders are incompatible with lithography processes and transport measurements, here we use a deliberately designed, homemade specimen holder that can load the SiO<sub>2</sub>/Si substrates suitable for FET nanodevice fabrication and operation. The SiO<sub>2</sub>/Si substrates are configured with microfabricated narrow slits with a width of ca. 5–20  $\mu\text{m}$  where the TEM electron beam will pass through to acquire the ED pattern of target nanotubes that suspend across the slit. A schematic diagram of our design is depicted in the Supporting Information (Figure S1) Horizontally aligned ultralong DWNTs were grown on the SiO<sub>2</sub>/Si slit substrates by ethanol CVD growth, following a procedure similar to that of the previously reported ultralong SWNTs.<sup>6,7</sup> The lengths of the individual DWNTs that suspend across the slits can normally be over 1 mm. As shown in Figure 1a, palladium (Pd) metal leads are evaporated on the nanotube with a “top-contact” manner in a region more than 10  $\mu\text{m}$  away from the slits so as to avoid any unpredictable influence on the electrical transport properties by electron irradiation.<sup>8</sup> After loading the slit substrate into the TEM specimen holder, ( $n$ ,  $m$ ) indices of the target DWNTs were first identified by ED across the slit (Figure 1c). Here we note that, although ED has now become

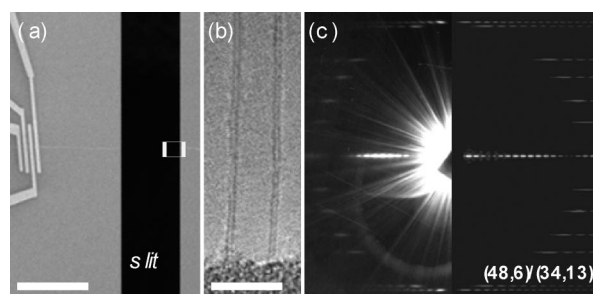


**Figure 1.** (a) A typical scanning electron micrograph of an isolated ultralong DWNT grown onto the SiO<sub>2</sub>/Si slit substrate. (b) High-resolution TEM image of the DWNT, acquired in the region as marked by the frame at the slit edge in panel a. (c) The corresponding ED pattern of the same DWNT (left, experimental; right, simulated). The ( $n$ ,  $m$ ) indices are identified as (48,6)/(34,13). Scale bars: (a) 10  $\mu\text{m}$ , (b) 5 nm.

a routine method for determining the ( $n$ ,  $m$ ) indices of SWNTs,<sup>9,10</sup> for DWNTs the accurate index assignment from an ED pattern is still difficult especially for tubes with relatively larger diameters. To solve this problem, we have developed a specialized method in the present study (see Supporting Information for details) that can enable an accurate ( $n$ ,  $m$ ) assignment of DWNTs from their respective ED patterns. After ED experiments, the electron beam was blacked out, and electrical measurements were performed on the selected nanotubes of interest in situ inside the TEM.

According to the different combinations of outer/inner tubes, DWNTs can be categorized into four types: metallic (M)/semiconducting (S), M/M, S/S, and S/M. Different from previous “chirality-blind” studies on DWNT-FETs,<sup>11,12</sup> it has now become possible in our work to accurately determine the ( $n$ ,  $m$ ) indices of each tube, thus enabling an unambiguous classification of the different types of DWNTs for systematic transport studies. Totally 82 DWNTs with the different chirality combination were investigated in this study. Shown in Figure 2a–d are a survey of typical transfer characteristics of the four types of DWNTs with chiral indices of (48,6)/(34,13), (22,19)/(19,12), (38,6)/(23,13), and (30,23)/(33,6), corresponding with chirality combination of M/M, M/S, S/S, and S/M, respectively. Their output characteristics are presented in Figure S5 (see Supporting Information). It can be seen that both the source-drain current ( $I_{\text{ds}}$ ) of the M/M and M/S DWNTs show no modulation by the gate voltage ( $V_{\text{g}}$ ), whereas the S/S DWNT exhibits the typical p-type semiconducting behaviors with on-/off-current ratio ( $I_{\text{on}}/I_{\text{off}}$ ) as high as  $10^4$ . As for the S/M DWNT, the source-drain current can be suppressed by a positive gate voltage but cannot be completely depleted, with the  $I_{\text{on}}/I_{\text{off}}$  being rather small (less than 20). Also, the on-off transition region of gate voltage has also been appreciably broadened, indicating the

<sup>†</sup> Chinese Academy of Sciences.

<sup>‡</sup> Peking University.

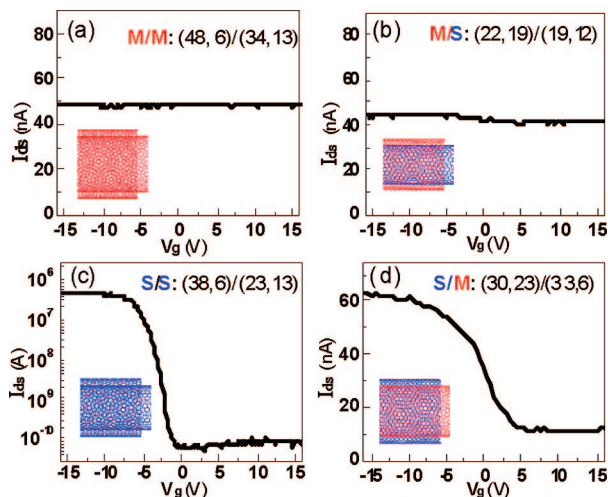


**Figure 2.** Representative transfer characteristics (current vs. gate-voltage) of the four types of DWNTs. (a) M/M DWNT with indices of (48,6)/(34,13); (b) M/S DWNT with indices of (22,19)/(19,12); (c) S/S DWNT with indices of (38,6)/(23,13); (d) S/M DWNT with indices of (30,23)/(33,6). The inset is the drawn atomic structure on the basis of the real ( $n$ ,  $m$ ) indices. The drain voltage ( $V_{ds}$ ) are 4, 4, 100, and 4 mV in panels a, b, c, and d, respectively.

low switching efficiency. As revealed by previous theoretical and experimental studies, in multiwalled carbon nanotubes in general, and in DWNTs in particular, the intershell interaction and coupling make a contribution to the overall transport characteristics of nanotubes.<sup>13–15</sup> And the distinct interaction between the outer and inner tubes should account for the difference in transfer characteristics of the four types of DWNTs.

Figure 3 shows  $I_{ds} - V_g$  curves of the FET made of the M/S type DWNT with chiral indices (45,15)/(28,24) before and after the

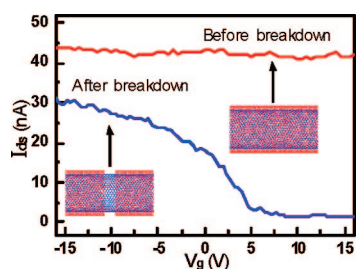


**Figure 3.** Transfer characteristics of a M/S type DWNT (45,15)/(28,24) before and after breaking down the outer tube. At the beginning, the current has no response to gate voltage (top curve). After applying a high current to break down the outer tube of DWNT, the transport exhibits a semiconducting behavior of the inner tube (bottom curve).

electrical breakdown of the outer tube (see Supporting Information, Figure S6). For the original DWNT, the current shows no dependence on the gate voltage; the DWNT demonstrates the typical metallic characteristic (top curve). To reveal the properties of the inner tube, we used a relatively higher current to break down the outer tube, and make the current access the inner tubes from the outer tubes by tunneling.<sup>16,17</sup> After breakdown, the transistor

properties of the DWNT changed remarkably. It can be seen that the current shows dependence on the gate voltage with  $I_{on}/I_{off} = 20$ , which exhibits a semiconducting characteristic of the inner tube (bottom curve). It is notable that the  $I_{on}/I_{off}$  is at least one order smaller than that of the pure semiconducting SWNTs with the similar diameter, it is due to that the screen effect of the remained metallic outer tube would decrease the field effect of the gate voltage.<sup>12</sup>

To sum up, chiral indices and chirality-dependent transport properties of DWNTs have been measured in situ on their field-effect transistors, through building DWNT-based FETs into TEM. The transport characteristics of DWNTs can be directly correlated with their chiral indices, and that of the inner tubes can also be accessed by in situ breaking down of the outer tubes. Probing the one to one relationship between electrical transport and chiral structure is a fundamental research for their chemical and physical applications.

**Acknowledgment.** This work is supported by the NSF (Nos. 50725209, 60621091, 20725307 and 50521201), MOST (Nos. 2007CB936203, 2007AA03Z353, 2006AA03Z402, 2006CB932403, 2006CB932602, 2006CB932701), and CAS of China. K. H. Liu acknowledges Mr. W. J. Ma for the helpful discussions.

**Supporting Information Available:** Materials and method, experimental setup, structural characterization, determination of chiral indices, output characteristics of FETs, and electrical breakdown of outer tubes. This material is available free of charge via the Internet at <http://pubs.acs.org>.

## References

- (1) Pfeiffer, R.; Pichler, T.; Kim, Y. A.; Kuzmany, H. in *Carbon Nanotubes: Advanced Topics in the Synthesis, Structure, Properties, and Applications*; Jorio, A., Dresselhaus, M. S., Dresselhaus, G., Eds.; Springer: New York, 2008; pp 495–530.
- (2) Kim, Y. A.; Muramatsu, H.; Hayashi, T.; Endo, M.; Terrones, M.; Dresselhaus, M. S. *Chem. Phys. Lett.* **2004**, *398*, 87.
- (3) Hayashi, T.; Shimanoto, D.; Kim, Y. A.; Muramatsu, H.; Okino, F.; Toyahara, H.; Shimada, T.; Miyauchi, Y.; Maruyama, S.; Terrones, M.; Dresselhaus, M. S.; Endo, M. *ACS Nano* **2008**, *2*, 485.
- (4) Jung, Y. C.; Shimamoto, D.; Muramatsu, H.; Kim, Y. A.; Hayashi, T.; Terrones, M.; Endo, M. *Adv. Mater.* **2008**, *20*, 4509–4512.
- (5) Kim, Y. A.; Muramatsu, H.; Park, K. C.; Shimamoto, D.; Jung, Y. C.; Kim, J. H.; Hayashi, T.; Saito, Y.; Endo, M.; Terrones, M.; Dresselhaus, M. S. *Appl. Phys. Lett.* **2008**, *93*, 051901.
- (6) Zhang, Y. Y.; Zhang, J.; Son, H. B.; Kong, J.; Liu, Z. F. *J. Am. Chem. Soc.* **2005**, *127*, 17156.
- (7) Yao, Y. G.; Li, Q. W.; Zhang, J.; Liu, R.; Jiao, L. Y.; Zhu, Y. T.; Liu, Z. F. *Nat. Mater.* **2007**, *6*, 283.
- (8) Vijayaraghavan, A.; Kanzaki, K.; Suzuki, S.; Kobayashi, Y.; Inokawa, H.; Ono, Y.; Kar, S.; Ajayan, P. M. *Nano Lett.* **2005**, *5*, 1575.
- (9) Amelinckx, S.; Lucas, A.; Lambin, P. *Rep. Prog. Phys.* **1999**, *62*, 1471.
- (10) Qin, L. C. *Rep. Prog. Phys.* **2006**, *69*, 2761.
- (11) Shimada, T.; Sugai, T.; Ohno, Y.; Kishimoto, S.; Mizutani, T.; Yoshida, H.; Okazaki, T.; Shinohara, H. *Appl. Phys. Lett.* **2004**, *84*, 2412.
- (12) Wang, S.; Liang, X. L.; Chen, Q.; Zhang, Z. Y.; Peng, L. M. *J. Phys. Chem. B* **2005**, *109*, 17361.
- (13) Uryu, S. *Phys. Rev. B* **2004**, *69*, 75402.
- (14) Hansson, A.; Stafstrom, S. *Phys. Rev. B* **2003**, *67*, 075406.
- (15) Yan, Q. M.; Wu, J.; Zhou, G.; Duan, W. H.; Gu, B. L. *Phys. Rev. B* **2005**, *72*, 155425.
- (16) Collins, P. G.; Hersam, M.; Arnold, M.; Martel, R.; Avouris, P. *Phys. Rev. Lett.* **2001**, *86*, 3128.
- (17) Huang, J. Y.; Chen, S.; Jo, S. H.; Wang, Z.; Han, D. X.; Chen, G.; Dresselhaus, M. S.; Ren, Z. F. *Phys. Rev. Lett.* **2005**, *94*, 236802.

JA808593V